3412–3428 *Nucleic Acids Research, 2018, Vol. 46, No. 7* *Published online 20 February 2018*
doi: 10.1093/nar/gky119

Combined cistrome and transcriptome analysis of SKI in AML cells identifies SKI as a co-repressor for RUNX1

Christine Feld[1,2,†], Peeyush Sahu[1,†], Miriam Frech[2], Florian Finkernagel[1], Andrea Nist[3], Thorsten Stiewe[3,4], Uta-Maria Bauer[1,*] and Andreas Neubauer[2,*]

[1]Institute of Molecular Biology and Tumor Research (IMT), School of Medicine, Philipps University Marburg, Hans-Meerwein-Str. 2, 35043 Marburg, Germany, [2]Department of Internal Medicine and Hematology, Oncology and Immunology, Philipps University Marburg, University Hospital Giessen and Marburg, Baldingerstr., 35043 Marburg, Germany, [3]Genomics Core Facility, Philipps University Marburg, Hans-Meerwein-Str. 3, 35043 Marburg, Germany and [4]Institute of Molecular Oncology, Philipps University Marburg, Hans-Meerwein-Str. 3, 35043 Marburg, Germany

Received November 27, 2017; Revised January 30, 2018; Editorial Decision February 01, 2018; Accepted February 09, 2018

ABSTRACT

SKI is a transcriptional co-regulator and overexpressed in various human tumors, for example in acute myeloid leukemia (AML). SKI contributes to the origin and maintenance of the leukemic phenotype. Here, we use ChIP-seq and RNA-seq analysis to identify the epigenetic alterations induced by SKI overexpression in AML cells. We show that approximately two thirds of differentially expressed genes are up-regulated upon SKI deletion, of which >40% harbor SKI binding sites in their proximity, primarily in enhancer regions. Gene ontology analysis reveals that many of the differentially expressed genes are annotated to hematopoietic cell differentiation and inflammatory response, corroborating our finding that SKI contributes to a myeloid differentiation block in HL60 cells. We find that SKI peaks are enriched for RUNX1 consensus motifs, particularly in up-regulated SKI targets upon SKI deletion. RUNX1 ChIP-seq displays that nearly 70% of RUNX1 binding sites overlap with SKI peaks, mainly at enhancer regions. SKI and RUNX1 occupy the same genomic sites and cooperate in gene silencing. Our work demonstrates for the first time the predominant co-repressive function of SKI in AML cells on a genome-wide scale and uncovers the transcription factor RUNX1 as an important mediator of SKI-dependent transcriptional repression.

INTRODUCTION

Acute myeloid leukemia (AML) is a heterogenous disease, which arises from hematopoietic progenitor cells by nuclear reprogramming. The underlying epigenetic alterations are causal for leukemia development and required for maintenance of the leukemic phenotype (1). Many patients display cytogenetic abnormalities that are important for treatment decision and prediction of prognosis. Chromosomal translocations are common genetic aberrations in AML and often involve hematopoietic transcription factors, such as RUNX1 and RARα, or transcriptional co-regulators, such as MLL (1). RUNX1 is essential for hematopoiesis and frequently altered in AML either by reciprocal chromosomal rearrangements, tandem duplications or point mutations (2,3). For example, in the AML-typical chromosomal translocation t(8;21), the RUNT domain of RUNX1 is fused to the almost entire ETO protein (also designated as RUNX1T1), therefore interfering with normal RUNX1 function and causing an oncogenic transcriptional response (4,5).

SKI was initially discovered as the cellular homologue of the transforming oncogene *v-SKI* found in the genome of multiple acutely transforming avian leukosis retroviruses (6,7). Importantly, in contrast to many other viral oncogenes, *SKI* does not require mutational activation, but SKI overexpression on its own is sufficient for acquiring transforming activity (8). In agreement with these findings, upregulated SKI expression was detected in various human tumors (5,9–11), including AML. The highest SKI expression was reported in the poor-prognosis AML subtype monosomy 7 or deletion 7q (-7/del7q) thereby leading to a differentiation block of leukemic cells (12). In search of the reason for this SKI upregulation, we identified miRNA29a

*To whom correspondence should be addressed. Tel: +49 6421 28 65325; Fax: +49 6421 28 65196; Email: bauer@imt.uni-marburg.de
Correspondence may also be addressed to Andreas Neubauer. Tel: +49 6421 58 66273; Fax: +49 6421 58 66358; Email: neubauer@staff.uni-marburg.de
†These authors contributed equally to the paper as first authors.

encoded at chromosome 7q32 as a potent repressor of SKI expression (13). Apart from its pathophysiological expression, SKI has been reported to be expressed at low levels in embryonic as well as adult hematopoietic stem cells (HSC) and to enhance HSC activity *ex vivo*, as uncovered in a gain of function screen (14–16). Enforced expression of SKI in murine hematopoietic stem and progenitor cells induced a gene signature associated with HSC characteristic and myeloid differentiation resulting in myeloproliferative disorder (17). The identification of SKI as a transforming viral oncogene together with the experimental evidence for the transforming activity of overexpressed SKI in the hematopoietic system classifies SKI as a leukemia-inducing oncogene.

SKI localizes to the nucleus, associates with chromatin and has been implicated in the regulation of different signaling pathways that control proliferation and differentiation (18). Although SKI does not directly bind to DNA on its own (19), it has been identified as a component of several DNA binding complexes (18). SKI regulates transcription mainly as a transcriptional co-repressor. Several modes of how SKI exerts its repressive function have been described, many of which require the interaction with transcription factors important for differentiation. The influence of SKI on TGFβ signalling is probably one of the best characterized pathways. Here, SKI directly interacts with the SMAD transcription factors SMAD2/3/4 and inhibits TGFβ signalling by recruiting the SIN3A co-repressor complex containing histone deacetylase (HDAC) activity to TGFβ responsive promoters, for example the *SMAD7* and *RORγt* gene promoter (20–26). Furthermore, SKI has been reported to compete with co-activators, such as the histone acetyltransferases CBP and p300, for binding to SMAD3 (20). Likewise, SKI modulates also other pathways, such as nuclear hormone receptor signalling, due to direct interaction with the co-repressor proteins N-CoR/SMRT and the concomitant recruitment of HDAC activity thereby triggering gene repression (12,27).

Although the different mechanisms of transcriptional repression by SKI have been well characterized, the epigenetic alterations induced by SKI overexpression and its global gene-regulatory contributions to myeloid leukemogenesis are still obscure. To address this issue in an unbiased manner, we generated CRISPR/Cas9-mediated deletion of SKI in HL60 cells and determined the genome-wide binding profile of SKI and the SKI-dependent transcriptome in leukemic cells. SKI knockout increased the myeloid differentiation potential of these cells in agreement with the oncogenic activity of SKI in AML. ChIP-seq and RNA-seq analyses performed in HL60 wild type and SKI-deficient cells showed that SKI executes a predominant transcriptional repressive function in leukemic cells. Gene Ontology analysis revealed that many of the differentially expressed genes are annotated to cellular processes, such as hematopoietic differentiation and inflammatory responses. Using motif enrichment analysis, we found that SKI ChIP peaks are enriched for the DNA binding consensus motif of important hematopoietic transcription factors, for example RUNX1. We further studied the yet unknown interaction of SKI and RUNX1. ChIP-seq for RUNX1 unraveled that nearly 70% of RUNX1 peaks overlap with SKI peaks and these common binding sites are enriched for enhancer regions. We identified common target genes of SKI and RUNX1 and a co-repressive function of SKI in RUNX1-mediated transcription. Together, these data demonstrate a novel mechanism of how SKI contributes to gene repression by cooperation with the transcription factor RUNX1 in AML cells.

MATERIALS AND METHODS

Cell lines and AML patient sample

HeLa and HEK293T cells were cultured in DMEM (Life Technologies) supplemented with 10% FCS. HL60 cells were maintained in RPMI (Life Technologies) supplemented with 10% FCS. Cells were purchased from DSMZ and regularly tested for mycoplasma contamination using a PCR-based method. Lentiviral transduced cells were selected and maintained in the presence of 0.5–1 μg/ml puromycin. For induction of doxycyline-inducible expression of shRNAs, cell culture medium was supplemented with 4 μg/ml doxycycline (Sigma-Aldrich). For ATRA (*all-trans* retinoic acid) treatment, HL60 cells were exposed to 1 μM ATRA for 2 d. Primary AML cells of a single patient were collected during leukapharesis, that was indicated due to the patient's symptoms, after informed consent.

Antibodies

The following antibodies were used: anti-SKI (sc-9140, Santa Cruz); anti-RUNX1 (ab23980, Abcam); anti-CDK2 (sc-163, Santa Cruz); anti-Flag (F3163, Sigma); anti-HA (HA.11 clone 16B12; Covance); anti-H3K4me3 (07-473, Millipore); anti-H3K27ac (39133, Active Motif); rabbit IgG (I5006, Sigma).

Plasmids

The following plasmids were used: pCMV-Tag2C-SKI (28), pCI-neo-SKI (Addgene), plasmids for HA-RUNX1 and Flag-RUNX1 (29), pGEX-RUNX1 full length (1-451) and deletion constructs (1-51; 51–177; 1–177; 177–451; 300–451) (29) and pGL3-hELA2 (30). For cloning of pInducer10-shRUNX1, shRNA-mir sequences including shRUNX1.1 (V2LHS_150257, 5′-CAAATGATCTGGTGGTTAT-3′), shRUNX1.2 (V3LHS_367631, 5′-AGGATACAAGGCAGATCCA-3′), shCON.1 (5′-CAGGAATTATAATGCTTATCTA-3′) and shCON.2 (5′-TCTCGCTTGGGCGAGAGTAAG-3′) were cloned via EcoRI/XhoI sites from pGIPZ vectors (Open Biosystems) into pInducer10 vector (31).

For design of sgRNA (single guide RNA), a web-based tool (http://crispr.mit.edu) was used and the following target sites in human *SKI* or GFP (as control=CTR) were chosen:

A (plus strand): 5′-CGAGCGCTGCGAGACCGTAC-3′
B (minus strand): 5′-CAGTACGGTCTCGCAGCGCT-3′
C (plus strand): 5′-ACCATCTCGTGCTTCGTGGT-3′
D (plus strand): 5′-CGAGACCATCTCGTGCTTCG-3′
E (plus strand): 5′-GGCCGCTTTCTCGGCGCGCT-3′
CTR (GFP): 5′-GGAGCGCACCATCTTCTTCA-3′

Pairs of oligos for these targeting sites (including the PAM sequence) were annealed and cloned into BsmBI-restricted lentiCRISPRv1 plasmid (Addgene), which allows bicistronic expression of Cas9 nuclease and sgRNA (32).

Transfections and infections

HeLa and HEK239T cells were transiently transfected using a standard $CaPO_4$ transfection protocol (for immunoprecipitation) or using Lipofectamine (Thermo Fisher) according to the manufacturer's protocol (for reporter gene assays). For production of lentivirus, HEK293T cells were transfected with the lentiviral expression plasmid and the two packaging plasmids pMD2.G and psPAX2 using XtremeGene (Roche). Supernatants containing viral particles were harvested 2 d after transfection and concentrated using PEG concentration. 5×10^5 HL60 cells were infected with virus upon addition of polybrene (8 μg/ml) via spinoculation (1200 rpm, 37°C, 1 h) and subsequently selected with 1 μg/ml puromycin. CRISPR/Cas9-mediated knockout pool cells expressing either one of the five different sgRNA targeting *SKI* A-E (SKI KO) or sgRNA targeting *GFP* (CTR) were analyzed for their genome targeting efficiency. Four *SKI*-specific sgRNAs (A, B, C and E) showed satisfying activity in T7 endonuclease assays (Supplementary Figure S1). Corresponding pool cells were then subjected to single cell cloning via serial dilution and screened for the loss of SKI expression by Western Blot and FACS analysis.

RNA isolation, reverse transcription quantitative PCR (RT-qPCR) and RNA-seq

Total RNA was prepared using RNA-Mini-Kit (Seqlab, Göttingen, Germany). For RT-qPCR, cDNA was synthesized using 0.8–1 μg of RNA, random hexamer oligonucleotides and MMLV (Thermo Scientific) according to the manufacturer's instruction. Then cDNA was subjected to PCR amplification using different primers (Supplementary Information, Text S1) and Absolute qPCR SYBR Green Mix (Thermo Scientific). For RNA-seq, libraries were prepared using TruSeq stranded mRNA Kit (Illumina) according to manufacturer's instructions.

Protein isolation and immunoprecipitation

For lysis, cells were resuspended in IPH400 buffer (50 mM Tris, pH 8, 400 mM NaCl, 5 mM EDTA, 0.5% NP40, protease inhibitors) and three times frozen and thawn. Cell extracts were diluted with same volume of IPH0 (50 mM Tris, pH 8, 5 mM EDTA, 0.5% NP40 protease inhibitors) and subjected to benzonase treatment in the presence of 7.5 mM $MgCl_2$ for 1–2 h at 4°C. For immunoprecipitation, cell extracts were diluted with IPH0 to a final concentration of 50 mM Tris, pH 8, 100 mM NaCl, 5 mM EDTA, 0.5% NP40. 650–700 μg of protein were precleared with 20 μl blocked Protein A Sepharose (1 mg/ml BSA) for 2 h at 4°C. Immunoprecipitation was performed overnight at 4°C with 4 μg of indicated antibodies. Subsequently, 20 μl of Protein A Sepharose were added for 2 h at 4°C. IPs were washed with IPH150 (50 mM Tris, pH 8, 150 mM NaCl, 5 mM EDTA, 0.5% NP40) and analyzed by SDS-PAGE and immunoblotting.

Chromatin immunoprecipitation quantitative PCR (ChIP-qPCR) and ChIP-seq

For chromatin immunoprecipitation (ChIP), cells were crosslinked for 10 min with 1% formaldehyde at room temperature. The reaction was stopped by addition of glycine 0.125 M for 5 min. Cell lysis was performed in lysis buffer I (5 mM PIPES pH 8, 85 mM KCl, 0.5% NP-40, protease inhibitors) for 20 min on ice. Cells were resuspended in lysis buffer II (10 mM Tris–HCl pH 7.5, 150 mM NaCl, 1% NP-40, 1% sodium deoxycholate, 0.3% SDS, 1 mM EDTA, protease inhibitors) and incubated on ice for 10 min. Chromatin was fragmented by sonification (50 × 3 s on ice at 25% amplitude for HL60, 40 × 3 s, 20% amplitude, Branson Sonifier W-250-D). For immunoprecipitations, chromatin was precleared with blocked Protein A Sepharose (1 mg/ml BSA and 400 μg/ml salmon sperm DNA) for 2 h at 4°C. Subsequently, 4 μg of the indicated antibodies were added to the chromatin and incubated overnight at 4°C. To immobilize immunoprecipitates, 50 μl of Protein A Sepharose were added for 2 h at 4°C. Then beads were washed twice with washing buffer I (20 mM Tris–HCl pH 8, 150 mM NaCl, 2 mM EDTA, 0.1% SDS, 1% Triton X-100), washing buffer II (20 mM Tris/HCl pH 8, 500 mM NaCl, 2 mM EDTA, 0.1% SDS, 1% Triton X-100), washing buffer III (10 mM Tris/HCl pH 8, 250 mM LiCl, 1 mM EDTA, 0.1% sodium deoxycholate, 1% NP-40) and TE buffer. Chromatin was eluted twice with 250 μl 0.1 M $NaHCO_3$ and 1% SDS for 15 min at RT. Crosslinking was reversed by incubation with Proteinase K and RNase for 3 h at 55°C following 65°C overnight. DNA was purified via QIAquick columns (QIAGEN) and either processed for ChIP-seq or analyzed by ChIP-qPCR using different primers (Supplementary Information, Text S1) and Absolute qPCR SYBR Green Mix (Thermo Scientific). For ChIP-seq, library was prepared according to the manufacturer's protocol (Diagenode, MicroPlex Library Preparation Kit).

Luciferase reporter assay

For reporter gene assays, 5×10^4 HEK293T cells were seeded per 24 well. The next day, 100 ng of reporter construct (pGL3-hELA2) was co-transfected with 300 ng of HA-RUNX1 Plasmid and varying amount of pCMV-Tag2C-SKI. In each transfection, 30 ng of a vector containing RSV-β-Gal reporter was co-transfected to normalize for transfection efficiency. Luciferase and β-galactosidase assays were performed 48 h post transfection as described before (33) and activities were measured using Mithras LB940 (Berthold Technologies).

Recombinant proteins and GST-pulldown experiments

GST and GST-tagged proteins were expressed in E.coli BL21 and bound to Glutathione beads (Protino Glutathione-Agarose 4B, Macherey-Nagel). Equal protein amounts were employed in pulldown experiments. *In vitro* transcription/translation (IVT) was performed using TNT

Coupled Reticulocyte Lysate Systems (Promega) using 2 μg of DNA template. 5 μl of IVT product was used per pulldown reaction and assay was performed as described by (34).

Flow cytometry

HL60 cell clones were stained with PE-labeled mouse anti-human CD11c (Clone B-ly6; BD Biosciences) for 30 min at 4°C and then washed with PBS. Subsequently, cells were stained with 2 μg/ml DAPI (4′,6-diamidino-2-phenylindole) for dead cell exclusion and measured with a LSR II flow cytometer (FACSDiva software version 6.1 from BD Biosciences). Data were analyzed with FlowJo version 7.6.5 (Tree Star).

Statistical analyses

All experiments were performed at least three times and each individual experiment in triplicates. Reproducible and representative data sets are shown. Error bars represent mean ± SD of triplicate reactions. Significance calculation on biological replicates ($n = 3$) were done using Welch's *t*-test and are shown in Supplementary Figures.

Bioinformatic analysis

ChIP-seq. Samples were sequenced as single-end reads using Illumina HiSeq 1500. Reads were demultiplexed and then aligned with Bowtie2 (35) against Homo sapiens, release-74, Ensembl genome. After alignment de-duplication was performed to remove multiple reads aligned to the same genomic start site. De-duplicated BAM files were used to visualize data and further analysis. Peak calling was performed using MACS 1.3.7 (36). All peaks were called accounting the background with respective IgG control ChIP-seq. Peaks were further filtered with criteria ≥35 tag counts and ≤2-fold enrichment above IgG and density based criteria (peak length/tag count ≤ 15). Peaks were annotated with the TSS of their nearest gene (regardless of distance). Human genome distribution of genomic regions (TSS, Intron, Exon, Upstream, Intergenic; in Figure 1C) was calculated by annotating each base pair in the human genome with TSS, Intron, Exon, Upstream or Intergenic region based on the criteria of all TSS ±1.5 kb, upstream –1.5 to –5 kb, intergenic > 5 kb, excluding the telomeric and centromeric repeat regions.

Heatmaps were created with custom script where read density data were extracted in 100 bp bin from –3 kb to +3 kb by keeping respective peak summit as center. To further investigate the structure in data, *k*-means clustering (distance metric = euclidean, number of cluster = 10, iterations = 1000) using python sklearn package was employed. In S-heatmaps (Figure 4A), SKI peaks with a maximum ±20 kb distance from the nearest TSS were selected and sorted in ascending order on distance from TSS. Next for selected SKI peaks, keeping the nearest TSS as the center read density data for –20 kb to +20 kb region was extracted in 200 bp bins. The read coverage was normalized to total read count and multiplied by million and plotted with R, heatmap3 package. Used published data were downloaded from Encode and ArrayExpress database in fastq format and further processed as mentioned above. Data was visualized using Integrative Genomics Viewer (IGV) (37). To find enriched DNA motifs within the SKI binding sites, we used MEME SUITE 4.10.2 (38). Sequences for analysis were extracted for ±100 bp and ±250 bp from SKI peak summit.

RNA-seq. Samples were sequenced in biological triplicate as single end reads using Illumina HiSeq 1500. Reads were aligned with Tophat2 (39) against Homo sapiens, release-74, Ensembl genome. Read coverage (number of overlapping reads per base pair) was calculated over non-overlapping exons. The exon counts were aggregated for each gene to build a read count table using SubRead function featureCount (40). Differentially regulated genes were calculated using DESeq2 (41). For differentially regulated genes a threshold (FC ≥ 2 or FC ≤ –2, P-val < 0.05) was followed. To analyze the biological significance of genes, Metascape (http://metascape.org) (42) was used for gene ontology analysis. In expression based gene binning (Figure 4B), first we removed all the genes having no expression in HL60 CTR-1 and KO-3 cells in all replicates. Then the remaining data set was normalized using Transcript Per Million (TPM) (43). Finally, we combined the three CTR-1 replicates using the mean of each gene and expression quantiles were estimated.

Gene set enrichment analysis (GSEA). Runx1-KO and Runt-OE mouse data (GSE40155) was downloaded and raw arrays were normalized using GCRMA package and differential gene expression was performed using limma package in R. Differentially regulated genes (FC ≥ 2 or FC ≤ –2, P-val < 0.05) were filtered and mouse gene names were converted to human gene names using biomaRt package in R for further comparison. Differentially regulated genes from Runx1-KO and Runt-OE were converted into GSEA (44,45) gene set file (*.gmt) according to tools instruction for calculating the enrichment of overlap with HL-60 SKI-KO de-regulated genes.

Clinical data (TCGA). AML patient data was downloaded from TCGA data portal (https://tcga-data.nci.nih.gov/docs/publications/laml_2012/) containing information on cytogenetic abnormality and mRNA expression (RNAseq). Patient samples with unknown or complex cytogenetic abnormality were filtered out. Data used was RPKM normalized. We extracted patient data from all used patient samples for the differentially regulated genes, which we had defined after SKI knockout in HL60 cells. This filtered patient data was joined with RPKM normalized data of HL60 CTR-1 cells. The combined data set was used to perform hierarchical clustering (linkage = ward, distance = Euclideam, correlation = cophenet) using scikit-learn a python.

External data. ChIPseq: H3K4me1: ERS420339 (ArrayExpress); Microarray Data: GSE40155; RNAseq Data: Clinical data: LAML_2012 (TCGA portal)

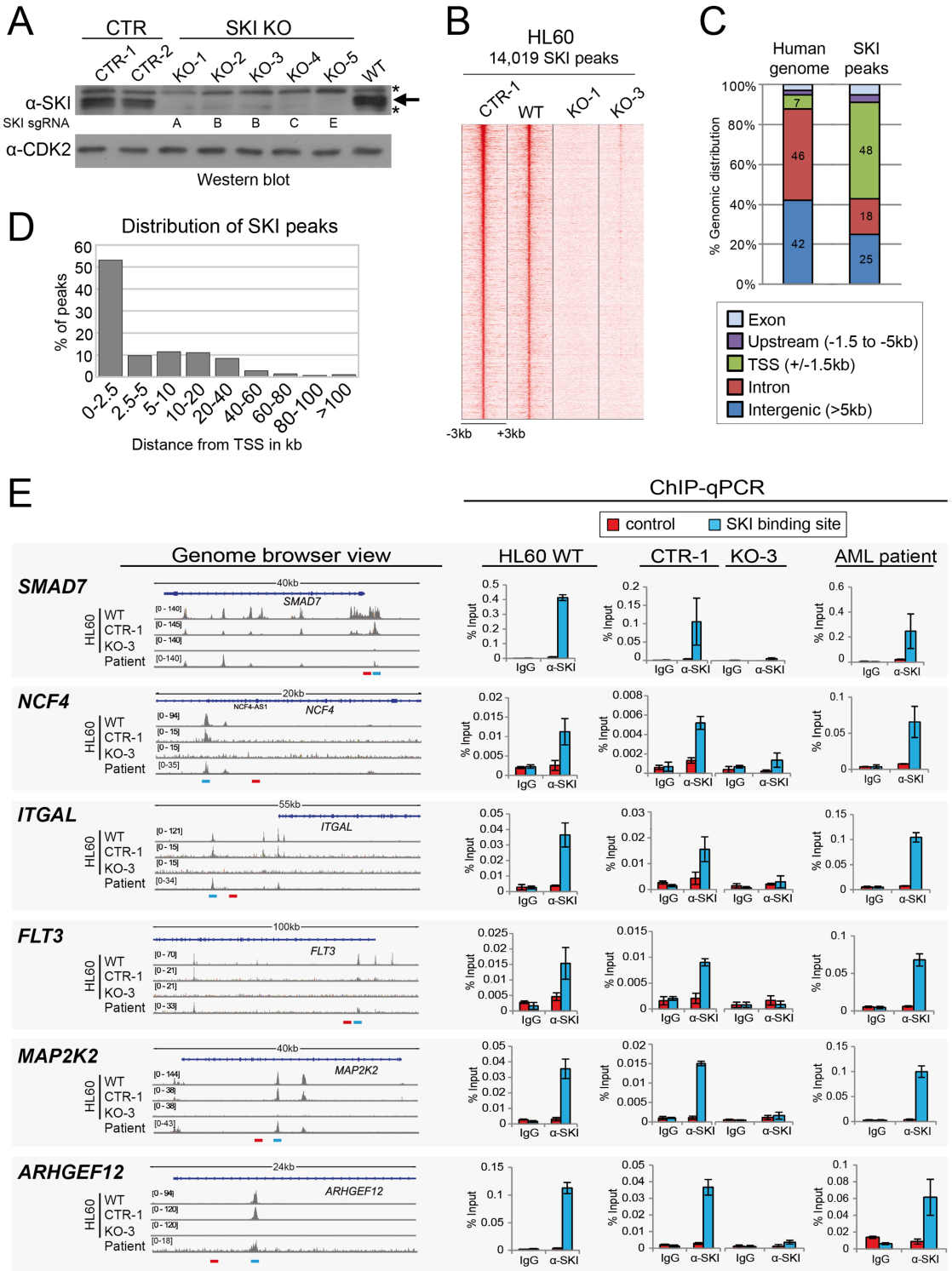

Figure 1. Genome-wide binding profile of SKI in AML cells. (**A**) Protein extracts from wild type (WT), control-deleted (CTR-1 and CTR-2) or SKI-deleted (KO-1 to KO-5) HL60 cell lines were analyzed by immunoblot using the indicated antibodies. Single guide RNAs targeting SKI (A, B, C and E), which were used to generate the SKI KO clones, are indicated: KO-1 with A, KO-2 and KO-3 with B, KO-4 with C, and KO-5 with E. The arrow indicates the SKI protein band; asterisks mark unspecific staining of the α-SKI antibody. CDK2 staining served as loading control. (**B**) Heatmap displays the comparison of SKI ChIP-seq enrichment for HL60 CTR-1, WT, KO-1 and KO-3 cells over the 14,019 CTR-1 binding sites sorted in descending order of their strength (±3 kb around the centered summits). (**C**) Genomic distribution of the SKI binding sites (of B) within the indicated genomic regions (exon, upstream, TSS, intron and intergenic) was compared to the distribution of these regions in the human genome. (**D**) Relative distribution of SKI binding sites is plotted according to their distance from TSS. (**E**) Genome browser views of the SKI ChIP-seq data sets of HL60 WT, CTR-1, KO-3 and AML patient cells are depicted for six gene loci (left). Standard ChIP assays were performed in HL60 WT, CTR-1, KO-3 and AML patient cells using control antibodies (IgG) and α-SKI (right). Precipitated DNA was analyzed by qPCR with primers amplifying the SKI binding site of the depicted loci as well as nearby control regions (respective primer amplicons are indicated in the genome browser views). Recruitment is displayed in % input of chromatin (mean ± SD of triplicates).

RESULTS

SKI binds to TSS as well as non-TSS regions in human AML cells

By combining analyses of genome-wide chromatin binding of SKI (ChIP-seq) and SKI-dependent transcriptome (RNA-seq) we aimed for a better understanding of how SKI contributes to leukemogenesis. Therefore we first established CRISPR/Cas9-mediated deletion of SKI in the AML cell line HL60, which exhibits elevated expression levels of SKI (data not shown). HL60 SKI knockout clones (KO-1 to KO-5) derived from four different sgRNA (single guide RNAs indicated in Figure 1A) upon single cell cloning. Selected SKI KO clones showed a complete loss of SKI expression compared to HL60 control clones (CTR-1 and CTR-2; generated using sgRNA targeting *GFP*) in immunoblot analysis (Figure 1A). 14,019 genomic binding sites of SKI were identified in HL60 CTR-1 cells by ChIP-seq analysis, which were compared to the SKI binding sites detected in HL60 WT cells (Figure 1B, Supplementary Figure S2). No major differences in the SKI peak profile between HL60 CTR-1 and WT cells were found, whereas SKI binding was lost in HL60 SKI KO cells (KO-1 and KO-3), as visualized in the heatmap showing the SKI ChIP signals sorted in descending order of their strength in HL60 CTR-1 cells in comparison to the other ChIP-seq data sets (Figure 1B). This analysis confirms that the 14,019 binding sites are SKI-dependent and specific.

Analysis of the relative distribution of SKI binding sites compared to the distribution of different genomic regions within the human genome unraveled that 78% of SKI peaks occur intragenic (upstream, TSS, intron and exon). Furthermore, they display a strong enrichment (53%) of regions located close to transcriptional start sites (TSS) (Figure 1C). When SKI binding sites were plotted based on their distance from TSS, we found that approximately 50% of total SKI peaks belong to a TSS/promoter fraction, and interestingly, a second enrichment was identified between 2.5–40kb distance from the TSS, accounting for a non-TSS fraction (Figure 1D). For validation of our ChIP-seq results, we selected candidate loci, of which six examples with their corresponding genes (*SMAD7*, *NCF4*, *ITGAL*, *FLT3*, *MAP2K2* and *ARHGEF12*) are depicted in genome browser views for HL60 WT, CTR-1 and KO-3 ChIP-seq data (Figure 1E). In independent ChIP-qPCR assays, we confirmed the SKI binding sites at these loci in HL60 WT, CTR-1 and CTR-2, whereas SKI deletion resulted in a loss of chromatin enrichment in HL60 KO cell lines (Figure 1E, Supplementary Figure S3). Additionally, primers amplifying a control region in proximity to the SKI binding sites revealed no SKI enrichment in HL60 WT or CTR cell lines and were unaffected by SKI knockout (Figure 1E, Supplementary Figure S3). The *SMAD7* gene promoter, for which we detected a SKI peak in HL60 cells, served as positive control, since this gene has been described before to be bound by SKI as a direct target of SKI-mediated repression (24). To investigate how the genomic SKI binding pattern in blast cells of AML patients with elevated SKI expression (data not shown) would relate to our findings in HL60 cells, we performed ChIP-seq analysis for SKI in such AML patient material. Interestingly, we detected a very similar binding profile of SKI in the blasts of the AML patient compared to HL60 cells (Supplementary Figure S4A, B) thus emphasizing the relevance of our findings in HL60 cells. Furthermore, browser views and ChIP-qPCR confirmed the validated SKI peaks of HL60 cells in the AML patient (Figure 1E). These results uncover for the first time the genome-wide binding profile of the oncoprotein SKI in an AML cell line as well as in AML patient cells. The predominant TSS and promoter proximal distribution of SKI evidences that the protein is likely involved in the regulation of gene expression on a genome-wide scale.

SKI predominantly functions as a transcriptional repressor in AML cells and its target genes are involved in immune cell differentiation and inflammatory responses

To characterize whether and how SKI might influence gene expression in AML, we determined the SKI-dependent transcriptome in HL60 cells by comparing RNA-seq profiles of HL60 CTR-1 and KO-3 cells. Thereby we identified 1,041 differentially expressed genes (Supplementary Figure S5A, B). Among the differentially expressed genes, 675 genes were up-regulated and 366 genes were down-regulated upon SKI deletion (Figure 2A). To identify potential direct target genes of SKI, we combined the RNA-seq and ChIP-seq data and found that 415 differentially expressed genes harbor SKI binding sites nearest to their TSS (Figure 2A). Among these genes, 283 were up-regulated and 132 were down-regulated indicating a predominant repressive function of SKI on global scale. In agreement with our findings (Figure 1E) and literature reports (24), SMAD7, a well-described SKI target gene, belonged to the subset of genes up-regulated upon SKI deletion, which we validated in the HL60 cell clones by independent RT-qPCR experiments (Figure 2B).

Next, we searched for pathways and cellular processes that associate with differentially expressed direct SKI target genes. Using Metascape (42) we identified terms associated with immune cell differentiation and inflammatory response overrepresented in up-regulated genes upon SKI deletion (Figure 2C). In contrast, the down-regulated genes were predominantly annotated to terms, such as negative regulation of developmental processes and transcriptional misregulation in cancer (Figure 2C). To verify these distinct subsets of differentially expressed genes we performed independent RT-qPCR assays in HL60 control cells (CTR-1 and CTR-2) and all SKI knockout cell lines (Figure 2D–G, Supplementary Figure S6). Up-regulated SKI target genes (depicted in red), which associate with gene functions of either immune cell differentiation (Figure 2D: *ITGAL*, *NCF4*, *MYCL*, *CCND1*) or inflammatory response (Figure 2E: *CCL5*, *CCL20*, *FAS, FCER1G, IL4R, IL2RB*, *HMOX1, PIK3R5*), showed elevated transcript levels upon SKI deletion compared to wild type conditions. Down-regulated targets (depicted in blue) were also validated (Figure 2F: *FLT3*, *AZU1*). Remarkably, the receptor tyrosine kinase gene *FLT3*, which is a frequently mutated oncogene in AML (46), belongs to the transcriptionally activated targets of SKI, representing a prime example for the gene annotation 'misregulation in cancer'. Furthermore, two examples of genes not affected in their transcriptional output by SKI

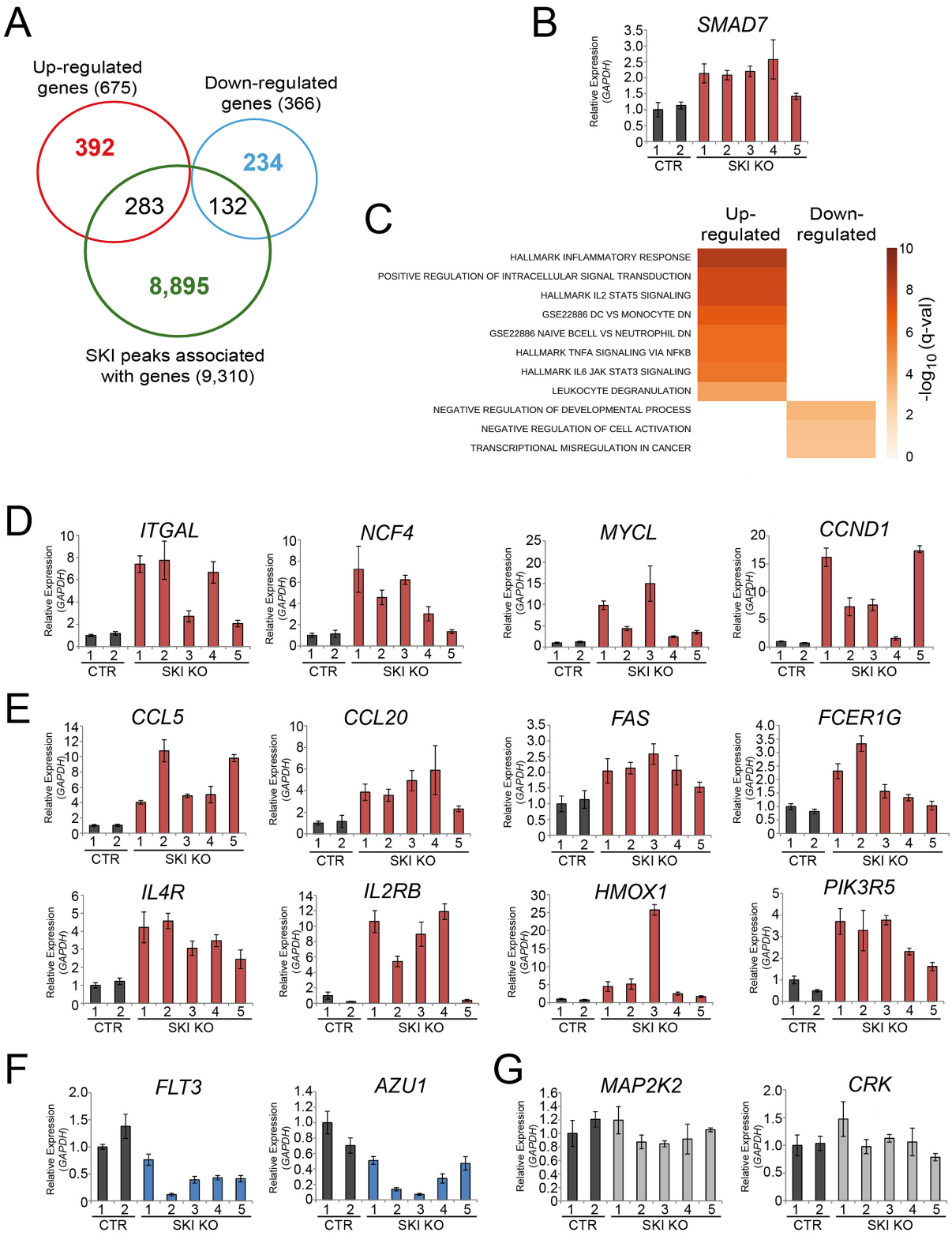

Figure 2. Predominant repressive function of SKI on target genes involved in hematopoietic cell differentiation and inflammatory response. (**A**) Venn diagram shows the intersection of differentially expressed genes upon SKI deletion (separated in up- and down-regulated genes) and genes associated with SKI binding site of HL60 CTR-1 cells. (**B**) Representative RT-qPCR analysis of *SMAD7* gene expression in HL60 CTR and SKI KO clones. Values were normalized to *GAPDH* and presented relative to CTR-1 (mean ± SD of triplicates). (**C**) Gene Ontology analysis using Metascape is shown for differentially expressed genes with SKI binding sites in their proximity. (**D–G**) Representative RT-qPCR analysis of selected genes in HL60 CTR and SKI KO cell clones. Genes were either up- (red; D, E), down- (blue; F) or unregulated (bright gray; G) upon SKI deletion in comparison to SKI wild type condition (dark gray). Values were normalized to *GAPDH* and presented relative to CTR-1 (mean ± SD of triplicates).

deletion were shown (Figure 2G: *MAP2K2*, *CRK*; depicted in gray). These results indicate that SKI acts on a genome-wide level predominantly as a transcriptional repressor and regulates important differentiation-associated, inflammatory and tumor-relevant pathways in leukemic cells.

SKI contributes to a myeloid differentiation block and the SKI-dependent transcriptome of HL60 cells resembles the gene expression signature of AML -7/7q subgroup

Given that SKI-deficient HL60 cells revealed transcriptional upregulation of immune cell differentiation markers, we examined next whether SKI contributes to the immature myeloid phenotype of HL60 cells. Differentiation of HL60 cells along the myeloid lineage is accompanied by distinct phenotypic alterations, such as the expression and exposure of the integrins CD11B and CD11C to the cellular surface. Utilizing RT-qPCR for *CD11B* in -/+ ATRA-treated HL60 cells (Figure 3A) and flow cytometry analysis for CD11C in untreated HL60 cells (Figure 3B), we determined the presence of these early maturation markers. In case of CD11B, we detected an enhanced ATRA-induced *CD11B* expression in the SKI knockout clones compared to control cells (Figure 3A, Supplementary Figure S7). In case of CD11C expression, we found low expression in HL60 control cells, whereas SKI knockout cells displayed increased levels of CD11C (Figure 3B). These observations indicate that SKI is involved in maintaining the differentiation block of HL60 cells, in line with its repressive function on differentiation-associated genes (Figure 2D, E). Additionally, these results corroborate our previous findings that overexpression of SKI leads to inhibition of ATRA-induced myeloid cell differentiation (12). Moreover, hierarchical clustering (47) comparing the SKI-dependent transcriptome of HL60 CTR cells (i.e. $\geq$2FC deregulated gene upon SKI-deletion) to gene expression profiles of published AML data sets, for which cytogenetics are available (48), identified several major clusters with respect to similarities in gene expression signature. Among these, HL60 CTR cells clustered in close proximity to AML –7/del7q (Figure 3C). This result reveals that the SKI-dependent transcriptome of HL60 cells resembles the gene expression signature of this AML subtype characterized by high SKI levels and bad prognosis (12), strengthening the significance of our findings in HL60 cells and identifying SKI as an important mediator of an aberrant transcriptional response in AML.

SKI chromatin binding at TSS and non-TSS regions induces epigenetic changes

Given that SKI cooperates for its gene-repressive functions with HDAC activity and leads to deacetylation of histones (12,20,21,24,27), we next examined whether SKI chromatin binding overlaps with certain histone modifications on a genome-wide level in leukemic cells. Therefore, we determined the distribution of H3K27ac, a histone H3 mark of active promoters as well as active enhancers, and H3K4me3, an active promoter mark, by ChIP-seq analysis in HL60 CTR-1 as well as HL60 KO-3 cells. Furthermore, we employed a published ChIP-seq data set of HL60 cells for H3K4me1 deposition, which marks primed enhancers and in conjunction with H3K27ac active enhancers (49). Then we plotted the enrichment levels of these three histone marks with respect to the SKI binding sites, which were sorted based on their distance from TSS over a region of 40kb from upstream to downstream. In agreement with our findings on the overall genomic SKI binding profile in HL60 cells (Figure 1C, D), we detected a high fraction of SKI peaks at or in close proximity to TSS (Figure 4A). Interestingly, this TSS fraction of SKI peaks co-occurs with high H3K4me3 and H3K27Ac levels suggesting that SKI is present at active promoters (Figure 4A). A second group of SKI peaks overlaps with H3K4me1 and H3K27Ac, indicating that these binding sites belong to enhancers primed or active for transcription (Figure 4A) and constitute a non-TSS fraction, as we have already postulated from Figure 1D.

Next, we analyzed the transcriptional output of genes with SKI peaks in their TSS/promoter or enhancer region. Therefore, genes were binned according to their transcriptional strength from no to high expression in 4 categories utilizing our RNA-seq data of HL60 CTR-1 cells. Genes belonging to the TSS/promoter fraction of SKI binding sites predominantly associated with highly transcribed genes, whereas enhancer-associated SKI sites were found in proximity to genes with overall lower transcription rate from medium to high expression (Figure 4B). To assess SKI-dependent expression changes within these two groups of SKI target genes, we revisited our analysis of differentially expressed genes upon SKI knockout (Figure 2A). We found deregulated genes in both groups, but genes with SKI binding sites in their enhancer were deregulated in much higher number (314 genes) compared to the TSS/promoter fraction of SKI target genes (101 genes), as illustrated in Figure 4C. Furthermore, we observed that target genes with SKI enhancer sites revealed an even more repressive influence of SKI than genes associated with TSS/promoter sites, since >70% of genes of the enhancer fraction were up-regulated upon SKI deletion (Figure 4C). These findings demonstrate that SKI executes functions in gene regulation both at TSS/promoter and enhancer sites in HL60 cells, however predominantly at enhancer sites and as a transcriptional repressor.

Next, we studied whether SKI would influence the deposition of H3 modifications and thereby would contribute to epigenetic changes in leukemic cells. We thus plotted the intensities of H3K27ac and H3K4me3, respectively, for SKI peaks (TSS as well as enhancer sites), which associate with deregulated genes. Up-regulated genes showed that the H3K27ac and H3K4me3 and levels significantly increased in SKI knockout cells compared to control HL60 cells (Figure 4D, E). In case of down-regulated genes, we found that H3K27ac levels are clearly decreased, whereas H3K4me3 levels showed only a slight decrease upon SKI deletion (Figure 4D, E). These effects on the deposition of active H3 marks are exemplified for the up-regulated target genes *CCL5*, *MYCL*, *NCF4*, *HMOX1* and the down-regulated target gene *FLT3* (Figure 4F). Furthermore, when we plotted fold change expression versus fold change of H3K27ac or H3K4me3 levels for the deregulated SKI target genes, we observed a positive correlation between SKI-mediated gene expression changes and enrichment levels of both marks (Supplementary Figure S8). Thus, our re-

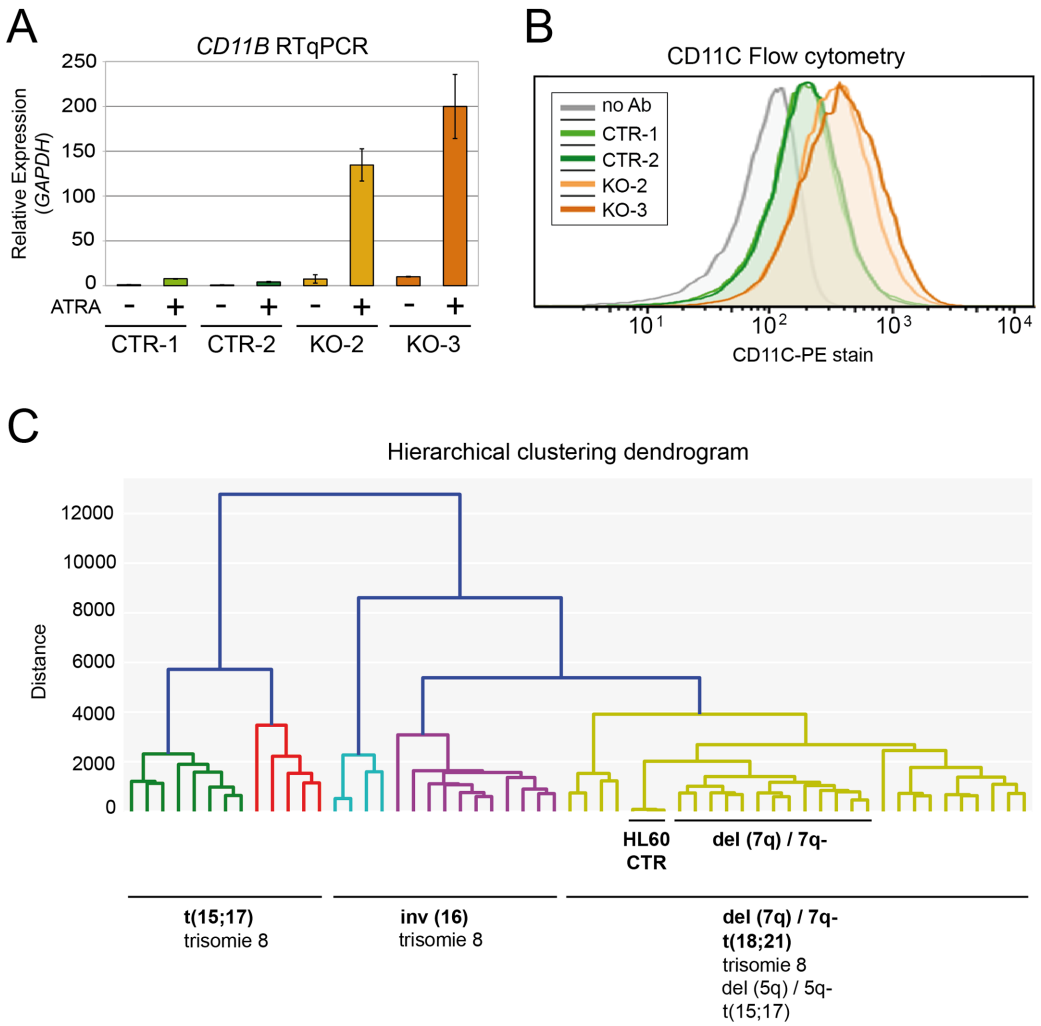

Figure 3. Similarity between the SKI-dependent gene expression signature of HL60 cells and the gene expression signature of AML subtype -7/7q. (**A**) Indicated HL60 cell clones were treated ± ATRA (1 μM) for 2 d and subsequently analyzed by RT-qPCR analysis for *CD11B* gene expression. Values were normalized to *GAPDH* and presented relative to untreated CTR-1 (mean ± SD of triplicates). (**B**) Expression of CD11C was analyzed in the indicated untreated HL60 cell clones by flow cytometry. Unstained HL60 cells (equal mixture of all four HL60 cell clones with no antibody) served as negative control. (**C**) Hierarchical clustering comparing the SKI-dependent transcriptome of HL60 CTR cells to gene expression profiles of published AML data sets containing various AML subgroups (48).

sults indicate that epigenetic alterations of H3K4me3 and H3K27ac levels positively correlate with the transcriptional effects of SKI in leukemic cells.

SKI binds together with important hematopoietic transcription factors

Since SKI does not directly bind to DNA (19), we performed an unbiased *de novo* motif enrichment analysis for the SKI binding sites using MEME Suite to identify transcription factors that potentially mediate SKI recruitment to chromatin in leukemic cells. Thereby we found that SKI peaks are enriched for consensus DNA binding motifs of well-known interaction partners of SKI, the transcription factors SMAD3/4 (24) and PU.1 (50), but importantly also for motifs of the hematopoietic transcription factors RUNX1 and CCAAT/enhancer binding protein CEBPβ, which have previously not been linked to SKI function (Supplementary Figures S9 and S10). To further narrow down the transcription factors potentially associated with SKI-bound regions of deregulated genes, we performed *de novo* motif analysis for exclusively these sites. Interestingly, we found that RUNX motifs were enriched at SKI peaks of up-regulated genes (Figure 5A). CEBP motifs were enriched at both up- and down-regulated target sites, whereas PU.1 and SMAD motifs were not enriched at these SKI peaks.

Given the prevailing gene-repressive function of SKI and the specific enrichment of RUNX motifs at repressed SKI targets, we concentrated in the following on the transcription factor RUNX1 as a novel potential cooperation partner of SKI. To examine whether and to which extent the binding of SKI and this predicted hematopoietic transcription factor would actually overlap, we performed ChIP-seq for RUNX1 in HL60 WT cells. RUNX1 binding was plotted based on centred SKI peaks, which were clustered depending on the associated H3 modification levels into TSS/promoter fraction (high H3K4me3/H4K27ac

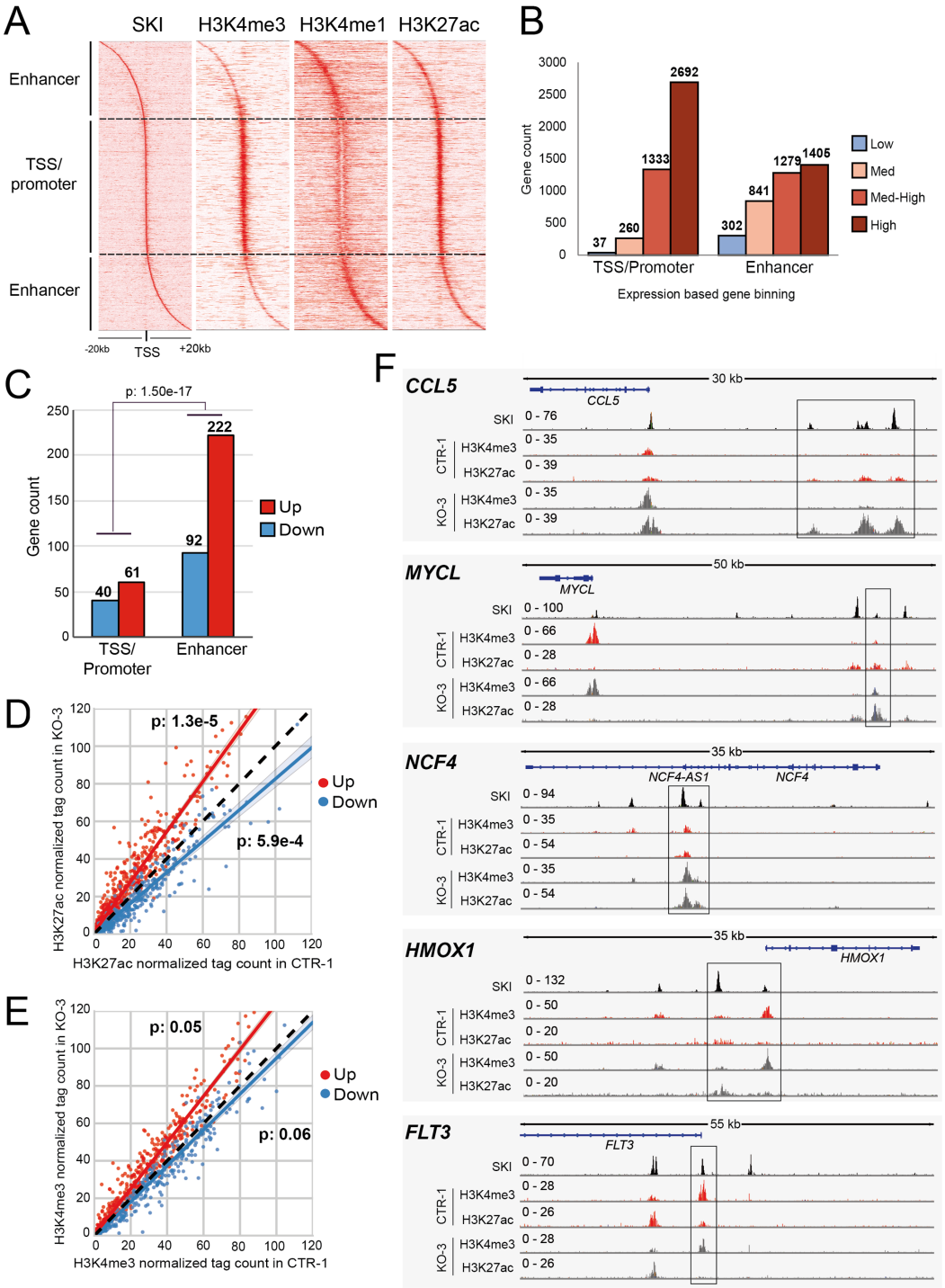

Figure 4. Correlation of SKI binding with the deposition of H3K4me3, H3K4me1 and H3K27ac. (**A**) Heatmap displays ChIP-seq enrichment levels of SKI and three histone marks (H3K4me3, H3K4me1 and H3K27ac) over 14,019 SKI binding sites (of CTR-1), which were sorted from upstream to downstream (±20 kb) based on their distance from TSS. (**B**) Genes associated either with TSS/promoter or enhancer SKI binding sites were binned according to the transcriptional strength (RNA-seq data of HL60 CTR-1 cells) in four categories from no to high based on expression quantiles (normalized as TPM = transcript per million): low <0.09 and ≥0; medium <0.84 and ≥0.09; medium-high <10.5 and ≥0.84; high >10.5. (**C**) Differentially expressed genes upon SKI knockout (at least fold change ±2 and *P*-val ≤ 0.05) were assigned as either up-regulated (red) or down-regulated (blue) and then the gene numbers with SKI bound at TSS/promoter or enhancer were plotted. *P*-value (Fisher's exact test) indicates that the number of de-regulated genes was significantly higher in the SKI enhancer-bound than in the SKI promoter-bound gene group. (**D**, **E**) Scatter plots present the normalized H3K27ac (D) and H3K4me3 (E) tag counts for up- (red fitted regression line) and down-regulated (blue fitted regression line) genes in HL60 CTR-1 versus KO-3 cells (FC $\log_2 = 0.75$, FDR < 0.05). Black dotted diagonals indicate identical levels of the respective histone marks in both cell lines. *P*-values (Welch's *t*-test) for the difference upon SKI knockout are indicated. (**F**) Genome browser views of SKI, H3K4me3 and H3K27ac ChIP-seq data sets of HL60 CTR-1 and KO-3 cells for gene loci are illustrated. *CCL5*, *MYCL*, *NCF4* and *HMOX1* serve as examples for up-regulated genes, and *FLT3* as an example for a down-regulated gene. Boxes highlight regions, where the deposition of H3K4me3 and/or H3K27ac is affected upon SKI deletion.

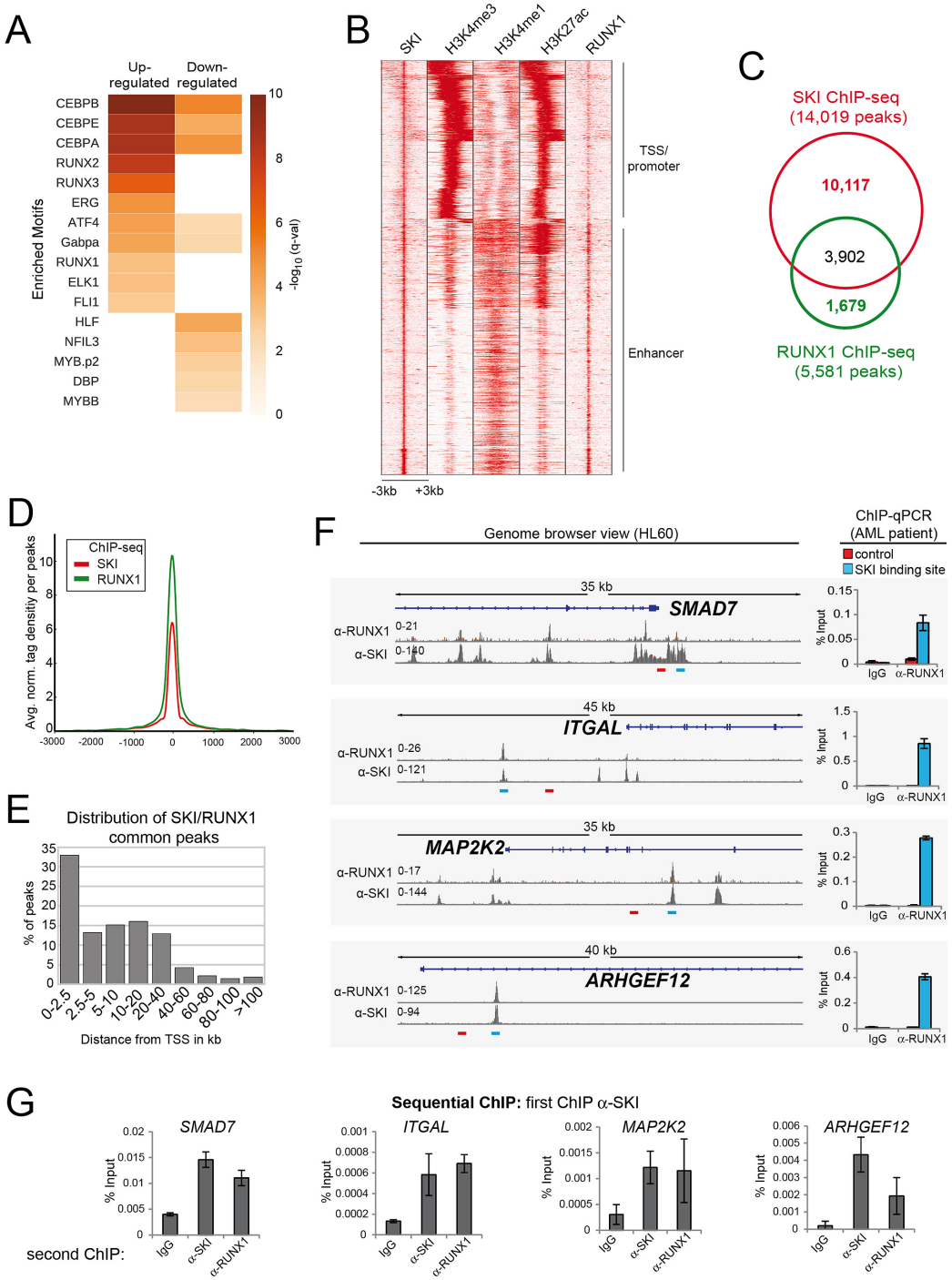

Figure 5. Overlap of SKI peaks with binding sites of important hematopoietic transcription factors. (**A**) *De novo* motif discovery analysis (MEME Suite) identified consensus binding sites of transcription factors in SKI peaks (±100 bp) of either up- or down-regulated genes, which are listed in the heatmap and coloured with respect to *q*-values. (**B**) Heatmap displays SKI ChIP signal over 14,019 sites in comparison to ChIP-seq profiles of histone marks (H3K4me3, H3K4me1 and H3K27ac) and the transcription factor RUNX1 in HL60 cells, with regions classified in TSS/promoter or enhancer (as indicated on the right) depending on the signal strength of their specific histone marks. (**C**) Venn diagram shows the intersection of peaks bound by SKI and RUNX1 in HL60 cells. (**D**) Cumulative tag density plot of SKI and RUNX1 ChIP-seq is shown for SKI/RUNX1 common binding sites. (**E**) Relative distribution of SKI/RUNX1 common binding sites is illustrated according to their distance from TSS. (**F**) Genome browser views of RUNX1 and SKI ChIP-seq data sets of HL60 WT cells are depicted for four gene loci (left). Independent, standard ChIP assays were performed in AML patient blast cells using control antibodies (IgG) and α-RUNX1 (right). Precipitated DNA was analyzed by qPCR with primers amplifying the SKI/RUNX1 common binding site of the depicted loci as well as nearby control regions (respective primer amplicons are indicated in the genome browser views). Recruitment is displayed in % input of chromatin (mean ± SD of triplicates). (**G**) Sequential ChIP assays (reChIP) were performed using in a first ChIP step α-SKI and subsequently immunoprecipitated chromatin was subjected to a second ChIP with isotype control IgG, α-SKI or α-RUNX1. Finally, precipitated DNA was analyzed by qPCR with primers amplifying the SKI/RUNX1 common binding site of the depicted loci (in F). Recruitment is displayed in % input of chromatin (mean ± SD of triplicates).

and low H3K4me1 levels) and enhancer fraction of SKI peaks (low H3K4me3, high H3K4me1 and medium/high H3K27ac levels) (Figure 5B). Interestingly, RUNX1 revealed a predominant occurrence at the enhancer sites of SKI. Comparison of the ChIP-seq profiles revealed a striking overlap between RUNX1 and SKI binding sites, as nearly 70% of the RUNX1 peaks also showed SKI enrichment in HL60 cells (Figure 5C). Similar results were obtained in the AML patient cells (Figure 1E), in which we performed RUNX1 ChIP-seq analysis and compared this data set to the SKI ChIP-seq data set derived from patient blasts (Supplementary Figure S11A–C). Cumulative tag density plot exhibited a perfect overlap of the binding summit of both proteins in HL60 cells (Figure 5D). In addition, analysis of the genomic distribution of SKI/RUNX1 common sites in HL60 cells displayed a more prominent enrichment for non-TSS regions (2.5–40 kb away from TSS) with >55%, compared to TSS enrichment with ∼33% of the common sites (Figure 5E). Using Fisher's exact test, we found SKI more frequently (*P*-value: 7.80e–298) associated with RUNX1 at enhancers than at TSS sites. This observation is also in agreement with our finding that RUNX1 shows a stronger enrichment at shared binding sites in enhancer regions (Figure 5B). Furthermore, we confirmed that RUNX1 is recruited to common SKI/RUNX1 binding sites in AML patient blast cells as well as HL60 WT cells using independent ChIP-qPCR assays for *SMAD7*, *ITGAL*, *MAP2K2* and *ARHGEF12* (Figure 5F, Supplementary Figure S12), which we already validated for SKI (Figure 1E). To address the question whether the two proteins would actually co-localize at the same genomic sites, we performed sequential ChIP (reChIP) experiments in HL60 cells followed by qPCR. Thereby, we found that SKI and RUNX1 co-occupy the same genomic sites in the regulatory regions of the *SMAD7*, *ITGAL*, *MAP2K2* and *ARHGEF12* gene (Figure 5G). These results suggest that RUNX1 mediates chromatin recruitment of SKI primarily to enhancer regions in leukemic cells.

SKI and RUNX1 cooperate via physical interaction in gene-repression of AML cells

Given that RUNX1 seems to be responsible for chromatin recruitment of SKI to a subset of target sites, we next examined whether SKI and RUNX1 would interact by performing co-immunoprecipitation analysis. Thereby, overexpressed Flag-tagged SKI and HA-tagged RUNX1 showed a specific interaction (Figure 6A). Reciprocal immunoprecipitation of endogenous SKI protein was found to co-purify overexpressed Flag-tagged RUNX1 (Figure 6B). Altogether these results demonstrate that both proteins physically interact in cell extracts. To map the interaction domain of SKI within RUNX1 we expressed recombinant SKI protein by IVT (*in vitro* transcription/translation) and performed pulldown experiments using bacterially expressed GST-RUNX1 full-length or deletion proteins (Figure 6C). RUNX1 protein is composed of the RUNT homology domain (RHD), which is responsible for DNA binding, and the transactivation domain (TAD), which modulates transcriptional activity and mediates interaction with several transcriptional co-regulators (51). GST-pulldown assays revealed that SKI predominantly binds to the C-terminus of RUNX1 (Figure 6C), which harbors the TAD domain, supporting the hypothesis that SKI is a novel co-regulator of RUNX1.

The fact that SKI binding sites, which associate with up-regulated genes upon SKI deletion, were enriched for RUNX binding motifs proposed that SKI might function as a co-repressor of RUNX1 and cooperate with RUNX1 in target gene repression. Comparison of SKI and RUNX1 ChIP-seq data identified 3,012 genes with SKI/RUNX1 shared binding sites in their proximity. Of these, 126 genes were up-regulated and 39 genes were down-regulated upon deletion of SKI (Figure 6D), indicating that the majority of genes deregulated and co-occupied by SKI and RUNX1 were repressed. To investigate the effect of SKI on RUNX1-mediated target gene transcription we performed reporter gene assays using the Elastase 2 gene promoter that has been reported to be activated by RUNX1 (30). Co-transfection of RUNX1 expression plasmid and Elastase 2 gene reporter plasmid in HEK cells revealed, as expected, an activation of the reporter gene, whereas additional co-expression of increasing amounts of SKI resulted in reduced reporter gene activation (Figure 6E, Supplementary Figure S13). SKI expression alone did not considerably influence the basal Elastase 2 gene reporter activity. These findings indicate a co-repressive function of SKI on RUNX1 mediated transcriptional activation of target genes. To study the impact of RUNX1 on SKI-repressed target genes in AML, we generated shRNA-mediated depletion of RUNX1 in HL60 cells. Depletion of RUNX1 resulted in enhanced transcription of the SKI targets *MYCL*, *HMOX1*, *SMAD7*, *IL4R*, *CCL5* and *IL2RB*, which contain common SKI/RUNX1 binding sites in their regulatory regions (Figure 6F, Supplementary Figure S14). These results suggest that RUNX1 mediates the chromatin recruitment of SKI to a subset of target genes and thereby enable SKI to execute its transcriptional repressive function in AML cells. This notion was further supported by Gene Set Enrichment Analysis (GSEA) (44,45). Here, we compared the differentially expressed genes upon SKI knockout in HL60 cells with gene sets obtained either from mice deficient in Runx1 or from mice overexpressing RHD, which possesses dominant negative effects (52). These analyses revealed a significant positive association between genes up-regulated in HL60 SKI knockout cells and genes up-regulated in the murine system upon knockout of Runx1 or overexpression of the RHD (Figure 6G, H). Altogether, these findings demonstrate that SKI and RUNX1 regulate a similar subset of target genes and support a functional cooperation of the two proteins in gene repression.

DISCUSSION

SKI is a transcriptional co-regulator overexpressed in AML and various other human tumors. Thereby SKI is thought to contribute to epigenetic alterations leading to the onset and maintenance of tumorigenesis. Given that the gene-regulatory roles of SKI overexpression have so far not been studied in an unbiased and genome-wide manner, we investigated here its genomic binding profile and the SKI-dependent transcriptome in AML cells either proficient

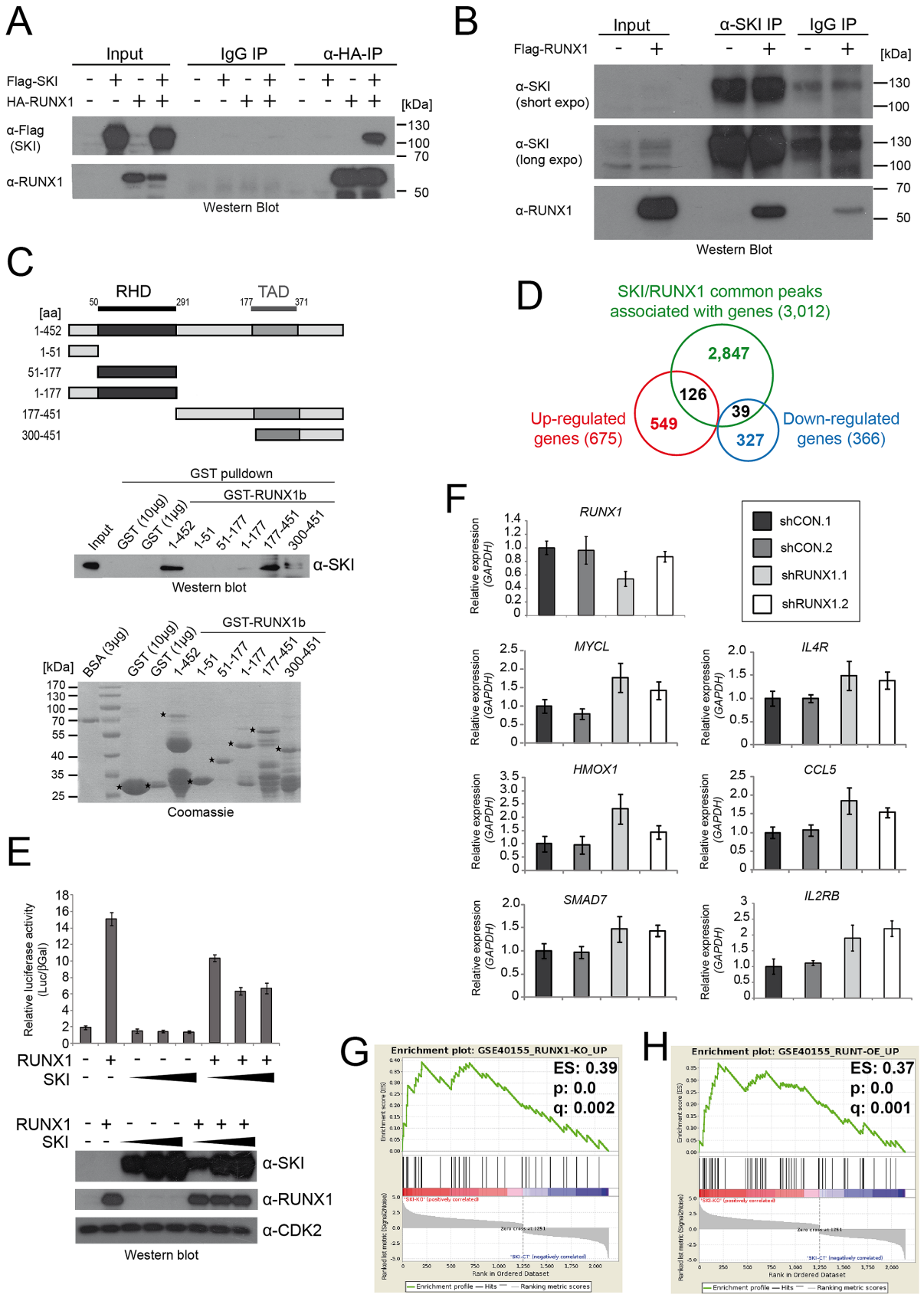

Figure 6. Cooperation of SKI and RUNX1 in gene repression of AML cells. (**A**) HeLa cells were transfected with empty vector, Flag-tagged SKI and HA-tagged RUNX1 constructs (alone or in combination, as indicated) and harvested 48 h post transfection. Protein extracts were subjected to immuno-

(HL60 CTR) or deficient in SKI (HL60 KO). Thus, we identified 14,019 SKI binding sites annotated with 9,310 unique genes. We found that SKI binding sites are enriched for TSS/promoter (high H3K4me3/H4K27ac and low H3K4me1 levels) as well as enhancer regions (low H3K4me3, high H3K4me1 and medium/high H3K27ac levels). This suggests that SKI exerts on a genome-wide scale co-regulator functions and conforms with previous work showing the presence of SKI at regulatory regions of individual gene loci (18). Among the genes with SKI peaks nearest to their TSS, 415 genes were differentially expressed upon SKI deletion revealing a potential direct transcriptional impact. The majority of SKI targets were not affected in their transcript levels by SKI knockout and might have acquired additional, more permanent chromatin states. For example, in case of silenced loci, DNA methylation or high-order chromatin structures might make the stable presence of SKI dispensable, similar to what has been reported for other co-regulators, such as the PRC complexes (53,54).

Interestingly, about two-thirds of all differentially expressed genes were up-regulated upon SKI deletion. Similarly, almost 70% (283 genes) of the differentially expressed, putative direct SKI targets were up-regulated demonstrating a predominant gene-repressive function of SKI in HL60 cells. This agrees with the reported co-repressor function of SKI, for example SKI-dependent inhibition of TGFβ signalling due to its interaction with SMAD transcription factors, for example leading to inhibition of Th17 cell differentiation due to repression of the *RORγt* gene locus (26). Furthermore, SKI has been described as a co-repressor of nuclear hormone receptor signalling by the thyroid hormone receptor (TRβ) and retinoic acid receptor (RARα) (12,27,55). SKI recruits co-repressor complexes, such as mSIN3A and N-CoR/SMRT, to these transcription factors, thus leading to HDAC-dependent direct transcriptional silencing of target genes. Remarkably, enhanced gene expression in HL60 KO cells was accompanied by increased levels of histone H3 acetylation (H3K27ac) at the corresponding SKI binding sites, whereas H3K4me3 levels were only slightly enhanced. This suggests that SKI deletion might lead to a concomitant loss of HDAC proteins from repressed target genes. Therefore, SKI seems to utilize also on genome-wide levels an HDAC-mediated repression mechanism.

Although SKI predominantly acts as a co-repressor, we found 30% of putative direct target genes to be down-regulated upon SKI deletion, indicating a gene-activating function of SKI. Consistent with this observation, SKI has been described to contribute to transcriptional activation, for example of muscle specific promoters/enhancers (56). Furthermore, transcription factors of the NFI-family mediate DNA recruitment of SKI in the context of gene activation (57). However, NFI binding motifs are not enriched in the SKI binding sites of our data set, suggesting that NFI-dependent recruitment might not be the mechanism how SKI exerts gene activation in HL60 cells. Whether SKI associates in different or similar co-regulator complexes at activated versus repressed target genes, is so far unsolved. *FLT3* gene that is frequently mutated in AML belongs to the activated SKI targets of our data set and was recently reported to be activated by the transcription factor SP1 in conjunction with the arginine methyltransferase PRMT5 in AML cells (58). Moreover, PRMT5 was found to participate in a 'yin-yang' manner in leukemic gene regulation, namely as co-activator as well as co-repressor (58). Remarkably similar to PRMT5, HDACs also display opposing functions in gene regulation as indicated by genome-wide distribution analysis of HDACs in thymocytes (59). At inactive but primed genes, HDACs function as transcriptional repressors and prevent premature transcriptional activity of these genes (59). At active genes, HDACs function as activators of transcription and are important to reset chromatin structures by histone deacetylation for the next round of transcription and for activating events sensitive to hyperacetylation (59–61). Interestingly, SKI, PRMT5 and HDAC3 have been show to constitute a protein complex in the context of SMAD-mediated repression of TGFβ-responsive promoters (24). Therefore, we speculate that SKI might act in AML cells similar to PRMT5 and HDACs in a bivalent fashion leading to gene activation as well as gene repression.

When we analyzed the differentially expressed SKI targets with respect to their association to the TSS/promoter or enhancer fraction of SKI binding sites, we observed deregulated expression in both groups upon SKI knockout. However, genes of the enhancer fraction were deregulated in

←

precipitation using α-HA antibodies for RUNX1 or isotype control IgG (IgG). Input (3%) and precipitates were analyzed by immunoblot using α-Flag (SKI) and α-RUNX1 antibodies. Size markers (in kDa) are shown on the right. (**B**) HEK293T cells were transfected with empty vector or Flag-tagged RUNX1 construct and harvested 48 h post transfection. Protein extracts were subjected to immunoprecipitation using α-SKI antibodies for endogenous SKI protein or isotype control IgG (IgG). Input (5%) and precipitates were analyzed by immunoblot using α-SKI and α-Flag (RUNX1) antibodies. Size markers (in kDa) are shown on the right. (**C**) GST-Pulldowns were performed using recombinant GST-RUNX1 (full-length or deletions, as depicted in the scheme upper panel; RHD = RUNT homology domain, TAD = Transactivation domain) and SKI expressed by *in vitro* transcription/translation (IVT). Input (20% IVT) and GST pulldown reactions were analyzed by immunoblot using α-SKI antibody (middle panel). Amounts of bead-bound GST-proteins were visualized by Coomassie staining. Asterisks mark the corresponding protein bands (lower panel). (**D**) Venn diagram shows the overlap of genes associated with SKI/RUNX1 common binding sites and genes differentially expressed upon SKI deletion. (**E**) For reporter gene assays, HEK293T cells were transiently transfected with 100 ng of luciferase reporter containing the Elastase2 gene promoter (pGL3-hELA2) and RSV-β-Gal reporter (the latter for normalization) -/+ expression plasmids for RUNX1 (300 ng) and SKI (increasing amounts: 25, 75 and 150 ng). 48 h post-transfection, cells were assayed for luciferase activity, of which mean values (± SD of triplicates) are shown relative to β-galactosidase activity (upper panel). SKI/RUNX1 overexpression was confirmed by immunoblot. CDK2 staining served as loading control (lower panel). (**F**) HL60 cells stably expressing doxycycline inducible control shRNAs (shCON.1, shCON.2) or shRNAs targeting RUNX1 (shRUNX1.1, shRUNX1.2) were treated with doxycycline for 7 d. RT-qPCR analyses were subsequently performed for a subset of SKI/RUNX1 common target genes. RT-qPCR for RUNX1 confirms the RUNX1 depletion. Values were normalized to *GAPDH* and presented relative to shCON.1 (mean ± SD of triplicates). (**G**, **H**) GSEA comparing genes regulated by Runx1 deletion in a conditional KO mouse model to genes differentially expressed after SKI deletion in HL60 cells (G)**.** GSEA comparing genes regulated by RHD overexpression in mouse (52) to genes differentially expressed after SKI deletion in HL60 cells (H).

much higher number and predominantly up-regulated, indicating that enhancer-bound SKI is primarily exerting co-repressive functions. Transcription factors that might mediate SKI chromatin recruitment in HL60 cells were identified by *de novo* motif enrichment analysis. SKI binding sites were enriched for consensus DNA binding motifs of known SKI interaction partners, such as SMAD3/4 and PU.1 (24,50), as well as novel putative interaction partners, such as RUNX1 and CEBP factors. Interestingly, SKI peaks of up-regulated genes, but not down-regulated genes upon SKI deletion, were enriched for RUNX1, implying that this transcription factor might specifically cooperate with SKI in gene-repression. ChIP-seq analysis revealed a significant overlap between chromatin binding of SKI and RUNX1. Given that RUNX1 was predominantly present at enhancer sites of SKI and uniquely enriched at repressed target genes, we focused on this novel putative connection between the two proteins.

RUNX1 is a master regulator of hematopoiesis and has been reported to drive the transcriptional network of blood cell development and terminal myeloid differentiation (62). RUNX1 itself acts as a weak transcriptional activator and requires the modulatory interaction with other transcription factors, such as GATA-1 and C/EBPα, or co-regulators, such as PRMT1 or p300, for strong and reliable transactivation capability (63–66). Transcriptional repression by RUNX1 is mediated by its interaction with co-repressors, such as mSin3A and PRMT6 (29,67). Strikingly, 70% of RUNX1 peaks overlapped with SKI peaks in HL60 cells. These SKI/RUNX1 common peaks show a predominant enrichment of enhancer regions. Sequential ChIP analysis and interaction assays suggest that RUNX1 might enable SKI recruitment to enhancer sites. Interestingly, the C-terminal TAD of RUNX1, which contains the interaction surface for several co-regulators (51), mediates the binding towards SKI indicating that SKI might modulate the transcriptional output of RUNX1. In agreement with this hypothesis, we found that SKI functions as a co-repressor of RUNX1 and that a subset of SKI/RUNX1 common target genes are indeed repressed by both proteins in HL60 cells. We therefore propose a novel mechanism by which SKI is recruited to chromatin via RUNX1 and both cooperate to regulate gene repression. GSEA comparing differentially expressed genes upon SKI deletion in HL60 cells with genes regulated by Runx1 deletion in conditional Runx1 KO mice or RHD overexpressing mice (52) corroborate this notion, as they showed a positive and significant enrichment of genes up-regulated upon SKI knockout and genes up-regulated in these murine models.

Genetic aberrations encompassing the *RUNX* gene locus belong to the most frequent mutations detected in AML. Best studied is the chromosomal rearrangement t(8;21), which fuses the RHD of RUNX1 to the almost entire ETO repressor protein, and therefore omits the TAD of RUNX1 (62). RUNX1-ETO competes with RUNX1 for DNA-binding and leads to global epigenetic changes, primarily repression, thereby causing a myeloid differentiation block in AML (68,69). We hypothesize that the interaction between SKI and RUNX1 also leads to a repressive complex. Consistently, genes up-regulated upon SKI deletion in HL60 cells were predominantly annotated to GO terms of hematopoietic cell differentiation and inflammatory responses. This suggests a function of SKI in the regulation of myeloid differentiation, which was further supported by our finding that SKI contributes to the immature myeloid phenotype of HL60 cells. Moreover, hierarchical clustering comparing the deregulated gene expression upon SKI deletion of HL60 cells to gene expression profiles of published AML dataset (48), revealed that the expression signature dependent on SKI and of AML –7/del7q resemble each other, indicating that SKI is a mediator of this aberrant transcriptional response.

Altogether, we identify for the first time the genome-wide binding sites of SKI in AML cells, which show enrichment for TSS/promoter and enhancer regions. Our work demonstrates a predominant transcriptional repressive function of SKI, primarily via enhancer-associated SKI. Finally, our work uncovers a functional link between SKI and RUNX1 and proposes a novel mechanism, by which SKI is recruited to chromatin through RUNX1 and cooperates with RUNX1 in gene repression of AML cells.

DATA AVAILABILITY

The data sets (ChIP-seq and RNA-seq) generated in this manuscript have been deposited on GEO with the Accession Number GSE107556.

SUPPLEMENTARY DATA

Supplementary Data are available at NAR Online.

ACKNOWLEDGEMENTS

We thank all members of the A.N. and U.M.B. laboratory, in particular Inge Sprenger, Christiane Rohrbach, Uta Wölfle and Daniele Fabellini, for their support during the work progress.

Author contributions: C.F. performed experiments, analyzed data, wrote the paper; P.S. analyzed data; M.F. performed experiments; F.F. analyzed data; A.N. performed experiments; T.S. analyzed data; U.M.B. analyzed data, wrote the paper; A.N. analyzed data.

FUNDING

Deutsche Forschungsgemeinschaft [TRR81/2 A03 to U.M.B., TRR81/2 A10 to T.S., BA 2292/1-3 to U.M.B., BA 2292/4-1 to U.M.B., STI 182/9-1 to T.S. and AN 310/18-1 to A.N.]; Deutsche José Carreras Leukämie-Stiftung [DJCLS R 13/17 to U.M.B. and AH06/01 to A.N.]. Funding for open access charge: DFG funding.

Conflict of interest statement. None declared.

REFERENCES

1. Elihu Estey,H.D. (2006) Acute Myeloid Leukaemia. *Lancet*, **368**, 1894–1907.
2. Wang,Q., Stacy,T., Binder,M., Marin-Padilla,M., Sharpe,A.H. and Speck,N.A. (1996) Disruption of the Cbfa2 gene causes necrosis and hemorrhaging in the central nervous system and blocks definitive hematopoiesis. *Proc. Natl. Acad. Sci. U.S.A.*, **93**, 3444–3449.

3. De Bruijn,M. and Dzierzak,E. (2017) Runx transcription factors in the development and function of the definitive hematopoietic system. *Blood*, **129**, 2061–2070.
4. Shima,Y. and Kitabayashi,I. (2011) Deregulated transcription factors in leukemia. *Int. J. Hematol.*, **94**, 134–141.
5. Takahata,M., Inoue,Y., Tsuda,H., Imoto,I., Koinuma,D., Hayashi,M., Ichikura,T., Yamori,T., Nagasaki,K., Yoshida,M. *et al.* (2009) SKI and MEL1 cooperate to inhibit transforming growth factor-β signal in gastric cancer cells. *J. Biol. Chem.*, **284**, 3334–3344.
6. Stavnezer,E., Gerhard,D.S., Binari,R.C. and Balazs,I. (1981) Generation of transforming viruses in cultures of chicken fibroblasts infected with an avian leukosis virus. *J. Virol.*, **39**, 920–934.
7. Li,Y., Turck,C.M., Teumer,J.K. and Stavnezer,E. (1986) Unique sequence, ski, in Sloan-Kettering avian retroviruses with properties of a new cell-derived oncogene. *J. Virol.*, **57**, 1065–1072.
8. Colmenares,C., Sutrave,P., Hughes Stephen,H. and Stavnezer,E. (1991) Activation of the c-ski oncogene by overexpression. *J. Virol.*, **65**, 4929–4935.
9. Heider,T.R., Lyman,S., Schoonhoven,R. and Behrns,K.E. (2007) Ski promotes tumor growth through abrogation of transforming growth factor-beta signaling in pancreatic cancer. *Ann. Surg.*, **246**, 61–68.
10. Chen,D., Lin,Q., Box,N., Roop,D., Ishii,S., Matsuzaki,K., Fan,T., Hornyak,T.J., Reed,J.A., Stavnezer,E. *et al.* (2009) SKI knockdown inhibits human melanoma tumor growth in vivo. *Pigment Cell Melanoma Res.*, **22**, 761–772.
11. Bravou,V., Antonacopoulou,A., Papadaki,H., Floratou,K., Stavropoulos,M., Episkopou,V., Petropoulou,C., Kalofonos,H. *et al.* (2009) TGF-β repressors SnoN and Ski are implicated in human colorectal carcinogenesis. *Cell. Oncol.*, **31**, 41–51.
12. Ritter,M., Kattmann,D., Teichler,S., Hartmann,O., Samuelsson,M.K., Burchert,A., Bach,J.P., Kim,T.D., Berwanger,B., Thiede,C. *et al.* (2006) Inhibition of retinoic acid receptor signaling by Ski in acute myeloid leukemia. *Leukemia*, **20**, 437–443.
13. Teichler,S., Illmer,T., Roemhild,J., Ovcharenko,D., Stiewe,T. and Neubauer,A. (2011) MicroRNA29a regulates the expression of the nuclear oncogene Ski. *Blood*, **118**, 1899–1902.
14. Phillips,R.L., Ernst,R.E., Brunk,B., Ivanova,N., Mahan,M.A., Deanehan,J.K., Moore,K.A., Christian Overton,G. and Lemischka,I.R. (2000) The genetic program of hematopoietic stem cells. *Science*, **288**, 1635–1640.
15. Forsberg,E.C., Prohaska,S.S., Katzman,S., Heffner,G.C., Stuart,J.M. and Weissman,I.L. (2005) Differential expression of novel potential regulators in hematopoietic stem cells. *PLoS Genet.*, **1**, e28.
16. Deneault,E., Wilhelm,B.T., Bergeron,A., Barabé,F. and Sauvageau,G. (2013) Identification of non-cell-autonomous networks from engineered feeder cells that enhance murine hematopoietic stem cell activity. *Exp. Hematol.*, **41**, 470–478.
17. Singbrant,S., Wall,M., Moody,J., Karlsson,G., Chalk,A.M., Liddicoat,B., Russell,M.R., Walkley,C.R. and Karlsson,S. (2014) The SKI proto-oncogene enhances the in vivo repopulation of hematopoietic stem cells and causes myeloproliferative disease. *Haematologica*, **99**, 647–655.
18. Bonnon,C. and Atanasoski,S. (2012) c-Ski in health and disease. *Cell Tissue Res.*, **347**, 51–64.
19. Nagase,T., Mizuguchi,G., Nomura,N., Ishizaki,R., Ueno,Y. and Ishii,S. (1990) Requirement of protein co-factor for the DNA-binding function of the human ski proto-oncogene product. *Nucleic Acids Res.*, **18**, 337–343.
20. Akiyoshi,S., Inoue,H., Kusanagi,K., Nemoto,N. and Chem,J.B. (1999) c-Ski acts as a transcriptional co-repressor in transforming growth factor-β signaling through interaction with Smads. *J. Biol. Chem.*, **274**, 35269–35277.
21. Luo,K., Stroschein,S.L., Wang,W., Chen,D., Martens,E., Zhou,S. and Zhou,Q. (1999) The Ski oncoprotein interacts with the Smad proteins to repress TGFbeta signaling. *Genes Dev.*, **13**, 2196–2206.
22. Xu,W., Angelis,K., Danielpour,D., Haddad,M.M., Bischof,O., Campisi,J., Stavnezer,E. and Medrano,E.E. (2000) Ski acts as a co-repressor with Smad2 and Smad3 to regulate the response to type β transforming growth factor. *Proc. Natl. Acad. Sci. U.S.A.*, **97**, 5924–5929.
23. Sun,Y., Liu,X., Eaton,E.N., Lane,W.S., Lodish,H.F. and Weinberg,R.A. (1999) Interaction of the Ski oncoprotein with Smad3 regulates TGF-β signaling. *Mol. Cell*, **4**, 499–509.
24. Tabata,T., Kokura,K., Ten Dijke,P. and Ishii,S. (2009) Ski co-repressor complexes maintain the basal repressed state of the TGF-beta target gene, SMAD7, via HDAC3 and PRMT5. *Genes Cells*, **14**, 17–28.
25. Denissova,N.G. and Liu,F. (2004) Repression of endogenous Smad7 by Ski. *J. Biol. Chem.*, **279**, 28143–28148.
26. Zhang,S., Takaku,M., Zou,L., Gu,A.D., Chou,W.C., Zhang,G., Wu,B., Kong,Q., Thomas,S.Y., Serody,J.S. *et al.* (2017) Reversing SKI–SMAD4-mediated suppression is essential for TH17 cell differentiation. *Nature*, **551**, 105–109.
27. Dahl,R., Kieslinger,M., Beug,H. and Hayman,M.J. (1998) Transformation of hematopoietic cells by the Ski oncoprotein involves repression of retinoic acid receptor signaling. *Proc. Natl. Acad. Sci. U.S.A.*, **95**, 11187–11192.
28. Zhao,H.L., Ueki,N., Marcelain,K. and Hayman,M.J. (2009) The Ski protein can inhibit ligand induced RARα and HDAC3 degradation in the Retinoic acid signaling pathway. *Biochem. Biophys. Res. Commun.*, **383**, 119–124.
29. Herglotz,J., Kuvardina,O.N., Kolodziej,S., Kumar,A., Hussong,H., Grez,M. and Lausen,J. (2012) Histone arginine methylation keeps RUNX1 target genes in an intermediate state. *Oncogene*, **32**, 2565–2575.
30. Lausen,J., Liu,S., Fliegauf,M., Lübbert,M. and Werner,M.H. (2006) ELA2 is regulated by hematopoietic transcription factors, but not repressed by AML1-ETO. *Oncogene*, **25**, 1349–1357.
31. Meerbrey,K.L., Hu,G., Kessler,J.D., Roarty,K., Li,M.Z., Fang,J.E., Herschkowitz,J.I., Burrows,A.E., Ciccia,A., Sun,T. *et al.* (2011) The pINDUCER lentiviral toolkit for inducible RNA interference in vitro and in vivo. *Proc. Natl. Acad. Sci. U.S.A.*, **108**, 3665–3670.
32. Shalem,O., Sanjana,N.E., Hartenian,E., Shi,X., Scott,D.A., Mikkelson,T., Heckl,D., Ebert,B.L., Root,D.E., Doench,J.G. *et al.* (2014) Genome-scale CRISPR-Cas9 knockout screening in human cells. *Science*, **343**, 84–87.
33. Kleinschmidt,M.A., Streubel,G., Samans,B., Krause,M. and Bauer,U.M. (2008) The protein arginine methyltransferases CARM1 and PRMT1 cooperate in gene regulation. *Nucleic Acids Res.*, **36**, 3202–3213.
34. Streubel,G., Bouchard,C., Berberich,H., Zeller,M.S., Teichmann,S., Adamkiewicz,J., Müller,R., Klempnauer,K.H. and Bauer,U.M. (2013) PRMT4 is a novel coactivator of c-Myb-dependent transcription in haematopoietic cell lines. *PLoS Genet.*, **9**, e1003343.
35. Langmead,B. and Salzberg,S.L. (2012) Fast gapped-read alignment with Bowtie 2. *Nat. Methods*, **9**, 357–359.
36. Zhang,Y., Liu,T., Meyer,C.A., Eeckhoute,J., Johnson,D.S., Bernstein,B.E., Nusbaum,C., Myers,R.M., Brown,M., Li,W. *et al.* (2008) Model-based analysis of ChIP-Seq (MACS). *Genome Biol.*, **9**, R137.
37. Robinson,J.T., Thorvaldsdóttir,H., Winckler,W., Guttman,M., Lander,E.S., Getz,G. and Mesirov,J.P. (2011) Integrative genome viewer. *Nat. Biotechnol.*, **29**, 24–26.
38. Bailey,T.L., Boden,M., Buske,F.A., Frith,M., Grant,C.E., Clementi,L., Ren,J., Li,W.W. and Noble,W.S. (2009) MEME Suite: Tools for motif discovery and searching. *Nucleic Acids Res.*, **37**, 202–208.
39. Kim,D., Pertea,G., Trapnell,C., Pimentel,H., Kelley,R. and Salzberg,S.L. (2013) TopHat2: accurate alignment of transcriptomes in the presence of insertions, deletions and gene fusions. *Genome Biol.*, **14**, R36.
40. Liao,Y., Smyth,G.K. and Shi,W. (2013) The Subread aligner: Fast, accurate and scalable read mapping by seed-and-vote. *Nucleic Acids Res.*, **41**, e108.
41. Love,M.I., Huber,W. and Anders,S. (2014) Moderated estimation of fold change and dispersion for RNA-seq data with DESeq2. *Genome Biol.*, **15**, 550.
42. Tripathi,S., Pohl,M.O., Zhou,Y., Rodriguez-Frandsen,A., Wang,G., Stein,D.A., Moulton,H.M., DeJesus,P., Che,J., Mulder,L.C.F. *et al.* (2015) Meta- and orthogonal integration of influenza 'oMICs' data defines a role for UBR4 in virus budding. *Cell Host Microbe*, **18**, 723–735.
43. Wagner,G.P., Kin,K. and Lynch,V.J. (2012) Measurement of mRNA abundance using RNA-seq data: RPKM measure is inconsistent among samples. *Theory Biosci.*, **131**, 281–285.
44. Mootha,V.K., Lindgren,C.M., Eriksson,K.F., Subramanian,A., Sihag,S., Lehar,J., Puigserver,P., Carlsson,E., Ridderstråle,M.,

Laurila,E. *et al.* (2003) PGC-1α-responsive genes involved in oxidative phosphorylation are coordinately downregulated in human diabetes. *Nat. Genet.*, **34**, 267–273.
45. Subramanian,A., Tamayo,P., Mootha,V.K., Mukherjee,S., Ebert,B.L., Gillette,M.A., Paulovich,A., Pomeroy,S.L., Golub,T.R., Lander,E.S. *et al.* (2005) Gene set enrichment analysis: A knowledge-based approach for interpreting genome-wide expression profiles. *Proc. Natl. Acad. Sci. U.S.A.*, **102**, 15545–15550.
46. Stirewalt,D.L. and Radich,J.P. (2003) The role of FLT3 in haematopoietic malignancies. *Nat. Rev. Cancer*, **3**, 650–665.
47. Pedregosa,F., Varoquaux,G., Gramfort,A., Michel,V., Thirion,B., Grisel,O., Blondel,M., Louppe,G., Prettenhofer,P., Weiss,R. *et al.* (2012) Scikit-learn: machine learning in python. *J. Mach. Learn. Res.*, **12**, 2825–2830.
48. The Cancer Genome Atlas Research Network. (2013) Genomic and epigenomic landscapes of adult de novo acute myeloid leukemia. *N. Engl. J. Med.*, **368**, 2059–2074.
49. Calo,E. and Wysocka,J. (2013) Modification of enhancer chromatin: what, how, and why? *Mol. Cell*, **49**, 825–837.
50. Ueki,N., Zhang,L. and Hayman,M.J. (2008) Ski can negatively regulates macrophage differentiation through its interaction with PU.1. *Oncogene*, **27**, 300–307.
51. Sood,R., Kamikubo,Y. and Liu,P. (2017) Role of RUNX1 in hematological malignancies. *Blood*, **129**, 2070–2082.
52. Matsuura,S., Komeno,Y., Stevenson,K.E., Biggs,J.R., Lam,K., Tang,T., Lo,M.-C., Cong,X., Yan,M., Neuberg,D.S. *et al.* (2012) Expression of the runt homology domain of RUNX1 disrupts homeostasis of hematopoietic stem cells and induces progression to myelodysplastic syndrome Expression of the runt homology domain of RUNX1 disrupts homeostasis of hematopoietic stem cells and induc. *Blood*, **120**, 4028–4038.
53. Bracken,A.P., Dietrich,N., Pasini,D., Hansen,K.H. and Helin,K. (2006) Genome-wide mapping of Polycomb target genes unravels their roles in cell fate transitions. *Genes Dev.*, **20**, 1123–1136.
54. Kirmizis,A., Bartley,S.M., Kuzmichev,A., Margueron,R., Reinberg,D., Green,D. and Farnham,P.J. (2004) Silencing of human polycomb target genes is associated with methylation of histone H3 Lys 27. *Genes Dev.*, **18**, 1592–1605.
55. Nomura,T., Khan,M.M., Kaul,S.C., Dong,H.-D., Wadhwa,R., Colmenares,C., Kohno,I. and Ishii,S. (1999) Ski is a component of the histone deacetylase complex required for transcriptional repression by Mad and thyroid hormone receptor. *Genes Dev.*, **13**, 412–423.
56. Engert,J.C., Servaes,S., Sutrave,P., Hughes,S.H. and Rosenthal,N. (1995) Activation of a muscle-specific enhancer by the Ski proto-oncogene. *Nucleic Acids Res.*, **23**, 2988–2994.
57. Tarapore,P., Richmond,C., Zheng,G., Cohen,S.B., Kelder,B., Kopchick,J., Kruse,U., Sippel,A.E., Colmenares,C. and Stavnezer,E. (1997) DNA binding and transcriptional activation by the Ski oncoprotein mediated by interaction with NFI. *Nucleic Acids Res.*, **25**, 3895–3903.
58. Tarighat,S.S., Santhanam,R., Frankhouser,D., Radomska,H.S., Lai,H., Anghelina,M., Wang,H., Huang,X., Alinari,L., Walker,A. *et al.* (2016) The dual epigenetic role of PRMT5 in acute myeloid leukemia: gene activation and repression via histone arginine methylation. *Leukemia*, **30**, 789–799.
59. Wang,Z., Zang,C., Cui,K., Schones,D.E., Barski,A., Peng,W. and Zhao,K. (2009) Genome-wide mapping of HATs and HDACs reveals distinct functions in active and inactive genes. *Cell*, **138**, 1019–1031.
60. Wang,A., Kurdistani,S.K. and Grundstein,M. (2002) Requirement of Hos2 histone deacetylase for gene activity in yeast. *Science*, **298**, 1412–1414.
61. Wagner,S., Weber,S., Kleinschmidt,M.A., Nagata,K. and Bauer,U.M. (2006) SET-mediated promoter hypoacetylation is a prerequisite for coactivation of the estrogen-responsive pS2 gene by PRMT1. *J Biol. Chem.*, **281**, 27242–27250.
62. Imperato,M.R., Cauchy,P., Obier,N. and Bonifer,C. (2015) The RUNX1–PU.1 axis in the control of hematopoiesis. *Int. J. Hematol.*, **101**, 319–329.
63. Elagib,K.E., Racke,F.K., Mogass,M., Khetawat,R., Delehanty,L.L. and Goldfarb,A.N. (2003) RUNX1 and GATA-1 coexpression and cooperation in megakaryocytic differentiation. *Blood*, **101**, 4333–4341.
64. Zhang,D.E., Hetherington,C.J., Meyers,S., Rhoades,K.L., Larson,C.J., Chen,H.M., Hiebert,S.W. and Tenen,D.G. (1996) CCAAT enhancer-binding protein (C/EBP) and AML1 (CBF alpha2) synergistically activate the macrophage colony-stimulating factor receptor promoter. *Mol. Cell. Biol.*, **16**, 1231–1240.
65. Zhao,X., Jankovic,V., Gural,A., Huang,G., Pardanani,A., Menendez,S., Zhang,J., Dunne,R., Xiao,A., Erdjument-Bromage,H. *et al.* (2008) Methylation of RUNX1 by PRMT1 abrogates SIN3A binding and potentiates its transcriptional activity. *Genes Dev.*, **22**, 640–653.
66. Kitabayashi,I., Yokoyama,A., Shimizu,K. and Ohki,M. (1998) Interaction and functional cooperation of the leukemia-associated factors AML1 and p300 in myeloid cell differentiation. *EMBO J.*, **17**, 2994–3004.
67. Lutterbach,B., Hou,Y., Durst,K.L. and Hiebert,S.W. (2000) A mechanism of repression by acute myeloid leukemia-1, the target of multiple chromosomal translocations in acute leukemia. *J. Biol. Chem.*, **275**, 651–656.
68. Ptasinska,A., Assi,S.A., Mannari,D., James,S.R., Williamson,D., Dunne,J., Hoogenkamp,M., Wu,M., Care,M., McNeill,H. *et al.* (2012) Depletion of RUNX1/ETO in t(8;21) AML cells leads to genome-wide changes in chromatin structure and transcription factor binding. *Leukemia*, **26**, 1829–1841.
69. Ptasinska,A., Assi,S.A., Martinez-Soria,N., Imperato,M.R., Piper,J., Cauchy,P., Pickin,A., James,S.R., Hoogenkamp,M., Williamson,D. *et al.* (2014) Identification of a dynamic core transcriptional network in t(8;21) AML that regulates differentiation block and self-renewal. *Cell Rep.*, **8**, 1974–1988.